Fermi National Accelerator Laboratory

FERMILAB-Pub-89/263-E
[E-772]

Test of Scaling of the Massive-Dihadron Cross Section*

D. M. Kaplan and R. Guo[a]
Northern Illinois University
DeKalb, Illinois 60115

C. N. Brown and W. E. Cooper
Fermi National Accelerator Laboratory
P.O. Box 500
Batavia, Illinois 60510

M. J. Wang
Case Western Reserve University
Cleveland, Ohio 44106

T. A. Carey, M. J. Leitch, P. L. McGaughey, C. S. Mishra,[b] J. M. Moss, and J.-C. Peng
Los Alamos National Laboratory
Los Alamos, New Mexico 87545

M. L. Barlett and G. W. Hoffmann
University of Texas
Austin, Texas 78712

December 1989

* Submitted to Phys. Rev. D

Test of Scaling of the Massive-Dihadron Cross Section

D. M. Kaplan and R. Guo[a]
Northern Illinois University, DeKalb, IL 60115

C. N. Brown and W. E. Cooper
Fermi National Accelerator Laboratory, Batavia, IL 60510

M. J. Wang
Case Western Reserve University, Cleveland, OH 44106

T. A. Carey, M. J. Leitch, P. L. McGaughey,

C. S. Mishra,[b] J. M. Moss, and J.-C. Peng
Los Alamos National Laboratory, Los Alamos, NM 87545

M. L. Barlett and G. W. Hoffmann
University of Texas, Austin, TX 78712

Measurements of the cross section for production of massive dihadrons by 800-GeV protons incident on a tungsten target are presented. These are compared with measurements taken at lower and higher $\sqrt{s}$ and with perturbative-QCD predictions. Scaling and A-dependence behaviors observed at lower energies are confirmed, and good agreement with QCD is obtained. Model dependences of earlier measurements are discussed.

In the late 1970's, the Columbia-Fermilab-Stony Brook (CFS) group studied production of pairs of high-transverse-momentum hadrons in collisions of 200-, 300-, and 400-GeV protons with beryllium and tungsten targets,[1-4] and the Columbia-CERN-Oxford-Rockefeller (CCOR) group studied production of π^0 pairs at the ISR.[5] We have taken new dihadron data using 800-GeV protons incident on a tungsten target. Comparing these new data with the lower-energy CFS and higher-energy CCOR samples, we find that the scaling behavior and A-dependence observed by CFS are corroborated at the higher energy, but that one of the CFS publications[1] contains a misleading figure.

We utilized the Fermilab E605/772 spectrometer (Figure 1), the details of which have been published previously[6]. For this run, we added a collimator at the exit of the "SM12" analyzing magnet, composed of 24" of copper followed by 48" of borated polyethylene, that restricted the vertical aperture to ± 10". 2.5×10^{10} protons per 20s beam pulse were incident on the face of a tungsten-disk target of thickness 3mm and diameter 3". Since the diameter of the target was much larger than the size of the beam, the targetting efficiency was 100%.

The beam flux was monitored by means of a secondary emission monitor (SEM) located in the beam line upstream of the target. The SEM has been calibrated several times in the last five years by comparing the SEM rate to the rate of production of ^{24}Na in copper foils; the calibration is found to be stable within $\pm 5\%$. Integrated proton fluxes are derived using a cross section[7] per Cu nucleus of 3.9 mb for the production of ^{24}Na. Note that the published CFS cross sections were based on a 10% lower value measured at Brookhaven[8], since measurements at Fermilab energies were not then available. We use this older value when comparing our results to those of CFS.

The data presented here satisfied a "low-bias" trigger which was prescaled by a factor of 8 or 16. The trigger required at least 60 GeV of energy deposition in the hadron calorimeter and coincident hits in three out of four hodoscope planes both on the left and right sides of the vertical centerline of the spectrometer. For 43,922 prescaled low-bias events written to tape, corresponding to 1.2×10^{11} incident protons, 3404 were found to contain two oppositely-charged hadron tracks after track reconstruction. These tracks were traced back through the magnetic field of SM12, and fiducial cuts were imposed to eliminate tracks passing too close to shielding material. The 2516 remaining pair events were cut on the vertical and horizontal positions at the target, to eliminate events due to upstream vacuum windows or the downstream beam dump. For each of the 437 remaining events, the intersection point of the track pair was computed in the y-z (magnetic bend) view and the x-z (non-bend) view. Figure 2 shows the distribution of these points along the z axis (incident

beam direction) in the two views. The target is seen clearly in both views. Figure 3 shows the mass and pair-p_t distributions of these events, and Figure 4 shows the pair-p_t distribution in two bins of mass: 5-6 GeV and 6-7 GeV.

Our efficiencies for recording and reconstructing these events are all high. Electronic dead time caused a 13.7% loss of beam. The trigger allowed any one of four hodoscope elements to be missing on each of the right and left sides, and the hodoscope counter efficiencies were all over 95%, so we make no correction for trigger counter efficiency. The calorimeter energy threshhold was well below the geometric turnon of the magnetic spectrometer acceptance (the lowest observed total momentum of a target-originated hadron pair was 90 GeV), so we make no correction for calorimeter trigger efficiency. The track reconstruction allowed up to seven of the 18 chamber planes to be missing (not more than three at any one of the three measurement stations), and the chamber efficiencies were all over 90%. The most likely number of planes per track was observed to be 17, and the measured reconstruction efficiency was 0.997 per track. We make no correction for tracking efficiency. At an early stage of analysis, events containing more than two tracks were eliminated from the data sample, amounting to 6% of events having two or more tracks. Since many of these events were probably not of target origin, we correct our cross sections upwards by 3% and assign a $\pm 3\%$ error contribution on the overall normalization to this source.

We compute the spectrometer acceptance by Monte Carlo simulation, using a dihadron production model which has been iterated to agree with the observed distributions. To convert these distributions into cross sections nevertheless requires some knowledge of the production distributions in regions not covered by our spectrometer. Figure 5 shows the spectrometer acceptance vs. mass, pair-p_t, center-of-mass rapidity, and dihadron-rest-frame (Collins-Soper) polar angle (θ^*). Like the CFS spectrometer, the E605/772 spectrometer covers only narrow regions in rapidity and polar angle, and its acceptance falls rapidly with increasing pair-p_t. We therefore follow the CFS convention and report cross sections differential in rapidity averaged over our rapidity interval. In comparing with CFS cross sections, we make the conventional assumption, appropriate to the production and decay into dihadrons of a hypothetical resonance, of isotropic distribution in $\cos\theta^*$. As an alternative we also present the cross section differential in $\cos\theta^*$. Since the acceptance vs. mass depends on the assumed p_t production distribution (larger for a narrow p_t distribution and smaller for a broad one), we consider first the invariant differential dihadron cross section vs. pair-p_t, which does not suffer from this model dependence. Figure 6a shows this cross section in two bins of mass.

To compare with 400-GeV CFS cross sections per beryllium nucleus, we scale ac-

cording to the linear nucleon-number (A) dependence which CFS observed.[2,4] We correct for our higher beam energy according to the CFS fit to the beam-energy dependence[4] $\sigma \propto (1 - m/\sqrt{s})^{13.0\pm0.4}$. Figure 7 compares the resulting cross sections with those of Reference 1, Figure 3. The agreement is quite good, verifying the p_t dependence observed by CFS as well as the s and A dependences.

We use a parametrization[9] of the observed CFS p_t dependence to compute the acceptance vs. mass (solid curve in Figure 5). Figure 6b gives the resulting cross section $d^2\sigma/dmdy$, averaged over our rapidity interval $-0.26 < y < 0.46$. In Figure 8, we compare this cross section, scaled as above for the s and A dependence, with that of Reference 1, Figure 2. The scaled 800-GeV data are in substantial disagreement with the CFS 400-GeV cross section (lower by a factor ranging from 10 at low mass to 3 at high mass). To develop some insight into this, we have also tried in the Monte Carlo a parametrization similar to that used by CFS[10] (which however is inconsistent with the CFS data), based on measurements at AGS energy[11]. The resulting acceptance, indicated by the dashed curve in Figure 5, is a factor of 2 to 3 lower at low mass but 30% higher at high mass than the acceptance computed above, with the two crossing over at $m \approx 6.5$ GeV. Since the CFS acceptance varied even more rapidly with p_t than does ours[4], we conclude that their sensitivity to the assumed p_t model was even greater, and this may explain the disagreement between our data and CFS.

We can compute a cross section which is less model dependent by restricting the pair-p_t and θ^* ranges. Figure 9 presents such a cross section, $d^3\sigma/dmdyd(\cos\theta^*)$, integrated over the range $0 < p_t < 1$ GeV and averaged over $-0.2 < \cos\theta^* < 0.2$. Also shown in the figure is the prediction of the QCD model of J. F. Owens[12], which was tuned to agree with the CCOR data, and which is seen to agree with our data as well.

We also compare our results directly to those of the CCOR group.[5] They measured the production of pairs of π^0's in proton-proton collisions at $\sqrt{s} = 44.8$ and 62.4 GeV at the ISR. They report a cross section differential in mass and rapidity and integrated over the range $p_t < 1$ GeV, $-0.4 < \cos\theta^* < 0.4$. Their observed $\cos\theta^*$ dependence is parametrized as $dN/d(\cos\theta^*) \propto (1 - \cos\theta^*)^{-a} + (1 + \cos\theta^*)^{-a}$, with $a = 2.97 \pm 0.05$, independent of mass and $\sqrt{s}$. We use this fit to extrapolate our cross section over their $\cos\theta^*$ range. The result is shown in Figure 10, plotted in the CCOR scaling form $m^{6.5}d^2\sigma/dmdy$, along with the CCOR data. Our data lie higher than CCOR's by about a factor of two, as would be expected from simple quark-counting arguments. We have also compared our data with preliminary results from Fermilab E711[13] covering the range 6 GeV$< m <$15 GeV, and we find excellent agreement in the region of overlap.

The new data confirm that the dihadron cross section near $y = 0$ and $p_t = 0$ shows

a simple scaling behavior with energy. The results differential (Figure 7) or restricted (Figure 9) in pair-p_t should have the smallest systematic normalization uncertainty, which we estimate to be $\pm 20\%$. Cross sections integrated over all p_t have greater uncertainty, due to the poorly known pair-p_t dependence at large p_t. This may help to explain the large discrepancy seen in Figure 8. We thank J. Owens, D. Levinthal, and J. Bjorken for useful discussions.

This work was supported in part by the U. S. Department of Energy.

---

[a]Present address: University of Illinois at Chicago, Chicago, IL 60680.

[b]Present address: Fermilab, Batavia, IL 60610.

[1]R. D. Kephart *et al.*, Phys. Rev. Lett. 39, 1440 (1977).

[2]R. L. McCarthy *et al.*, Phys. Rev. Lett. 40, 213 (1978).

[3]R. J. Fisk *et al.*, Phys. Rev. Lett. 40, 984 (1978).

[4]H. Jöstlein *et al.*, Phys. Rev. D **20**, 53 (1979).

[5]A. L. S. Angelis *et al.*, Nucl. Phys. B209, 284 (1982).

[6]Y. B. Hsiung *et al.*, Phys. Rev. Lett. 55, 457 (1985); J. A. Crittenden *et al.*, Phys. Rev. D 34 2584, (1986); D. M. Kaplan, "Production of Hadrons and Leptons at High p_t and Pairs at High Mass", in **VIIth Vanderbilt Conference on High Energy Physics: Quarks, Strings, Dark Matter, and All the Rest**, R. S. Panvini and T. J. Weiler, *eds.*, World Scientific, Singapore, 1987, p. 83.

[7]S. Baker *et al.*, Nucl. Instr. Meth. 222, 467 (1984).

[8]J. Hudis *et al.*, Phys. Rev. 129, 434 (1963) and J. B. Cumming *et al.*, Phys. Rev. C 14, 1554 (1976).

[9]$dN/dp_t \propto p_t\ e^{-[p_t^2/b(m)]}$, $b(m) = 1.27(0.16m^2 - 1.23m + 3.48)^2$.

[10]R. D. Kephart, private communication.

[11]$dN/dp_t \propto p_t\ e^{-bT}$, where $T \equiv \sqrt{m^2 + 1.5p_t^2} - m$, from J. J. Aubert *et al.*, Phys. Rev. Lett. 35, 639 (1975). Following CFS, we choose b = 1.6.

[12]J. F. Owens, private communication, and in **Proceedings of the Storrs Meeting,**

K. Haller *et al., eds.*, World Scientific, Singapore, 1989, p. 570.

[13]K. Streets, Ph.D. dissertation, Florida State University, 1989.

FIG. 1. Schematic diagram of the E605/772 spectrometer.

FIG. 2. Reconstructed z_{target} distributions in magnetic bend (y-z) and non-bend (x-z) views.

FIG. 3. Distribution of observed events vs. mass and pair-p_t.

FIG. 4. Event distributions vs. pair-p_t: a) $5 < m < 6$ GeV, b) $6 < m < 7$ GeV.

FIG. 5. Spectrometer acceptance vs. a) mass (for two assumed p_t distributions, see text), b) pair-p_t ($5 < m < 6$ GeV), c) pair-p_t ($6 < m < 7$ GeV), d) center-of-mass rapidity, e) cosine of Collins-Soper-frame polar angle.

FIG. 6. Differential cross sections vs. a) pair-p_t and b) mass.

FIG. 7. Comparison of invariant cross section for hadron-pair production vs. pair-p_t from this experiment, scaled as described in text, with that of CFS (ref. 1).

FIG. 8. Comparison of differential cross section for hadron-pair production vs. mass from this experiment, scaled as described in text, with that of CFS (ref. 1).

FIG. 9. Triply-differential cross section for hadron-pair production vs. mass. The curve is the prediction of the QCD model of J. F. Owens (ref. 12).

FIG. 10. Comparison of differential cross section for hadron-pair production vs. mass from

this experiment, scaled as described in text, with that of CCOR (ref. 5).

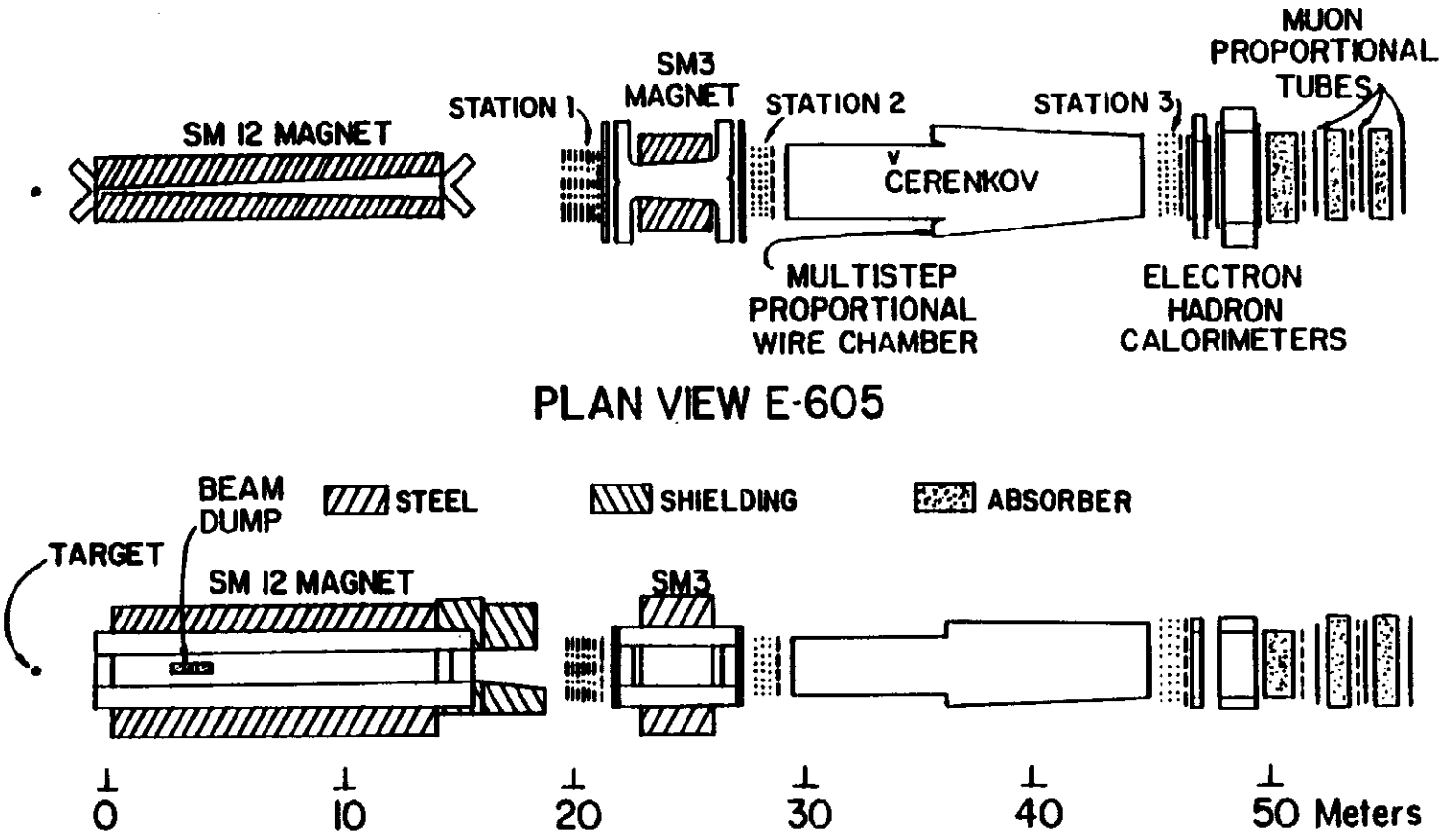
SM 12 MAGNET
STATION 1
SM3
MAGNET
STATION 2
CERENKOV
STATION 3
MUON
PROPORTIONAL
TUBES
MULTISTEP
PROPORTIONAL
WIRE CHAMBER
ELECTRON
HADRON
CALORIMETERS
PLAN VIEW E-605
BEAM
DUMP
STEEL
SHIELDING
ABSORBER
TARGET
SM 12 MAGNET
SM3
0
10
20
30
40
50 Meters
ELEVATION SECTION E-605
DRIFT CHAMBER
PROPORTIONAL CHAMBER
COUNTER BANK

Figure 1

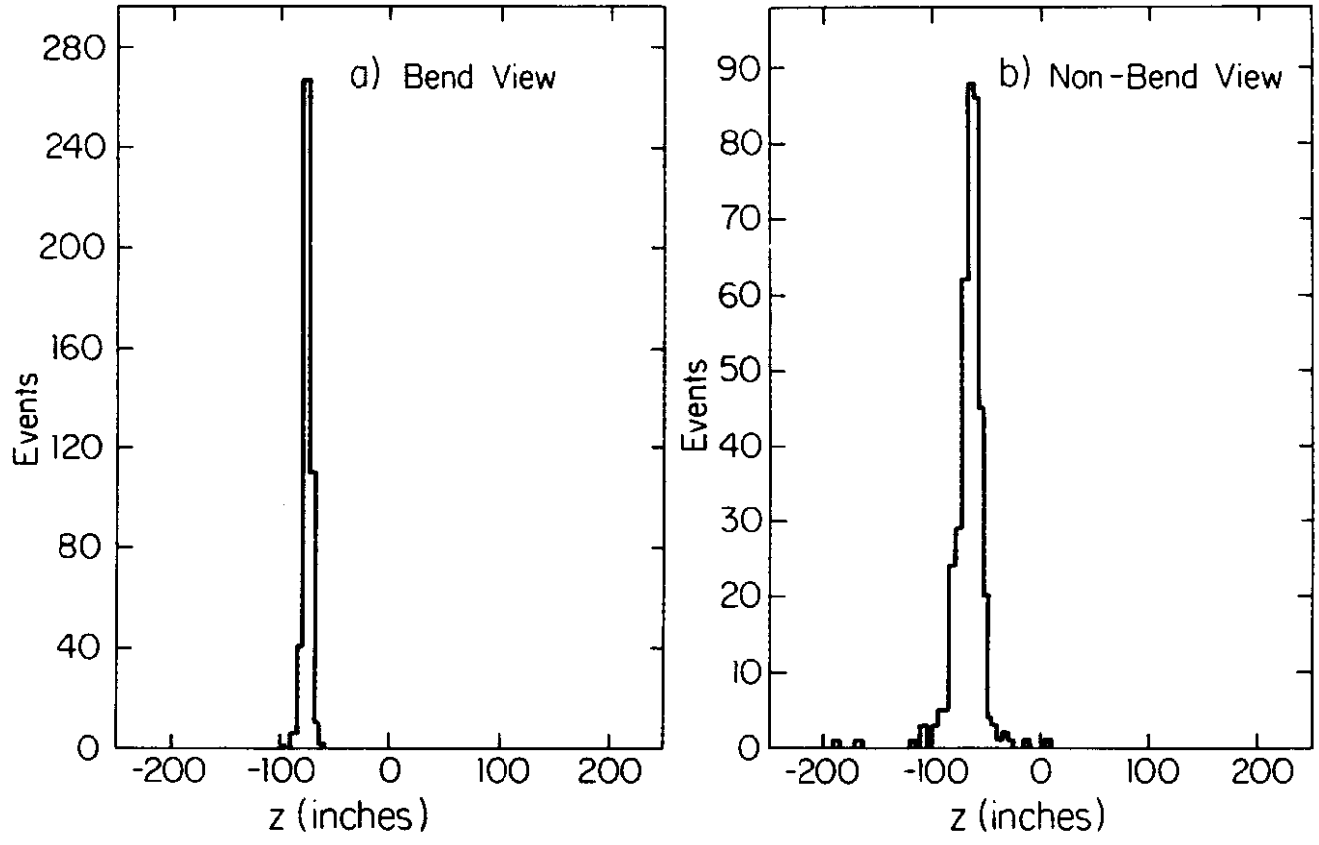
a) Bend View
b) Non-Bend View
Events
z (inches)
280
240
200
160
120
80
40
0
90
70
60
50
30
20
10
-200
-100
100
200

Figure 2

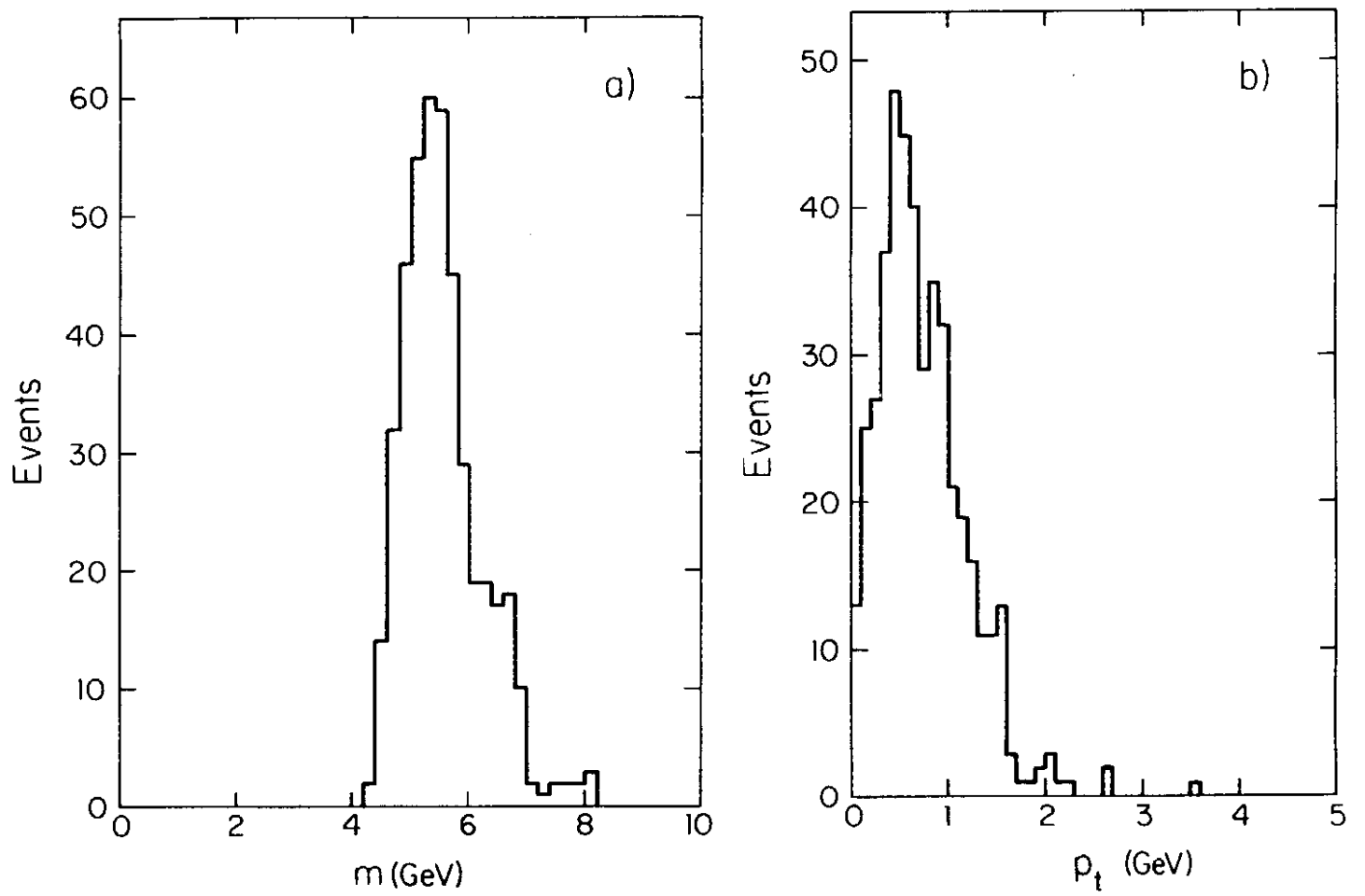
a)
Events
m (GeV)
0
10
20
30
40
50
60
0
2
4
6
8
10
b)
Events
p_t (GeV)
0
10
20
30
40
50
0
1
2
3
4
5

Figure 3

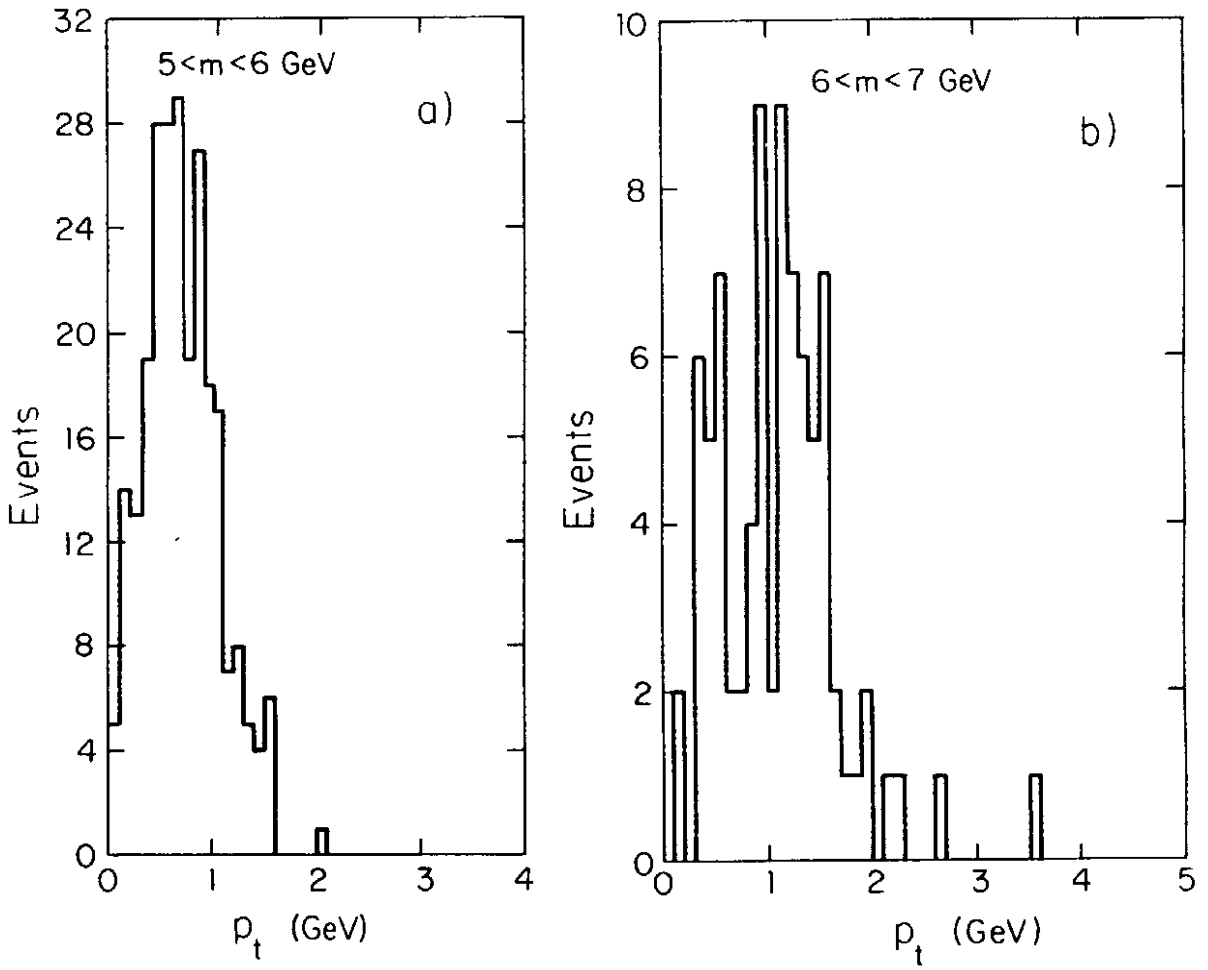

Figure 4

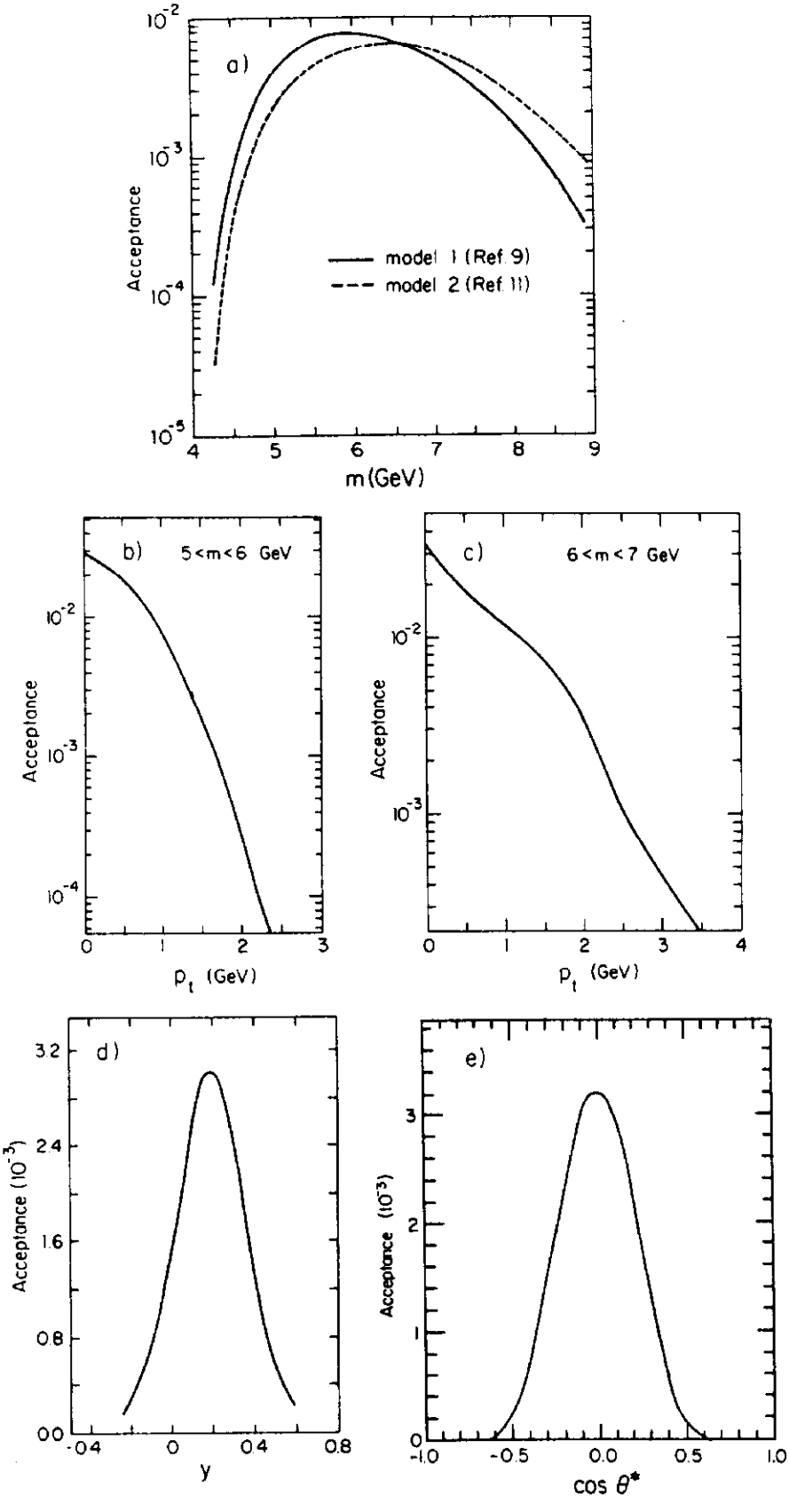
a)
Acceptance
model 1 (Ref. 9)
model 2 (Ref. 11)
m(GeV)
b) 5<m<6 GeV
Acceptance
p_t (GeV)
c) 6<m<7 GeV
Acceptance
p_t (GeV)
d)
Acceptance (10^{-3})
y
e)
Acceptance (10^{-3})
cos θ^*

Figure 5

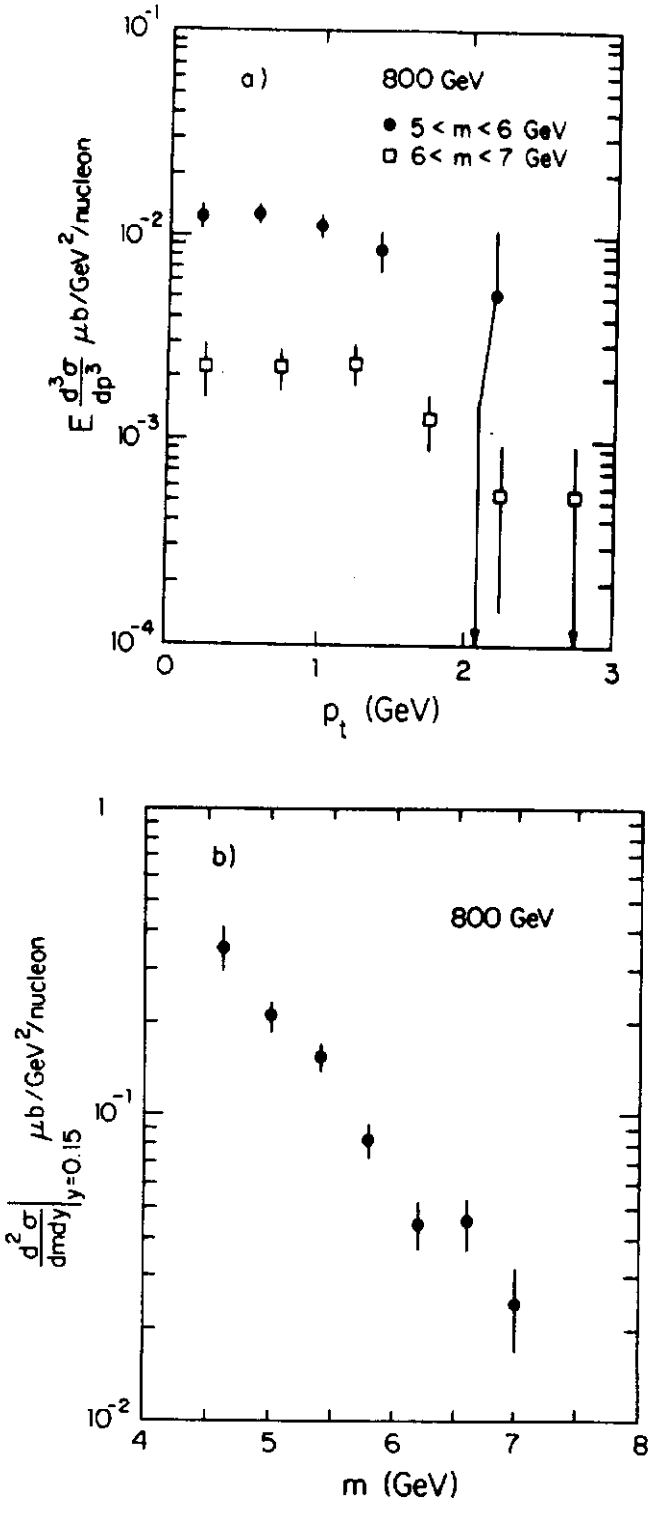
a)
800 GeV
● 5 < m < 6 GeV
□ 6 < m < 7 GeV
$E\frac{d^3\sigma}{dp^3}$ μb/GeV²/nucleon
p_t (GeV)
b)
800 GeV
$\frac{d^2\sigma}{dmdy}\Big|_{y=0.15}$ μb/GeV²/nucleon
m (GeV)

Figure 6

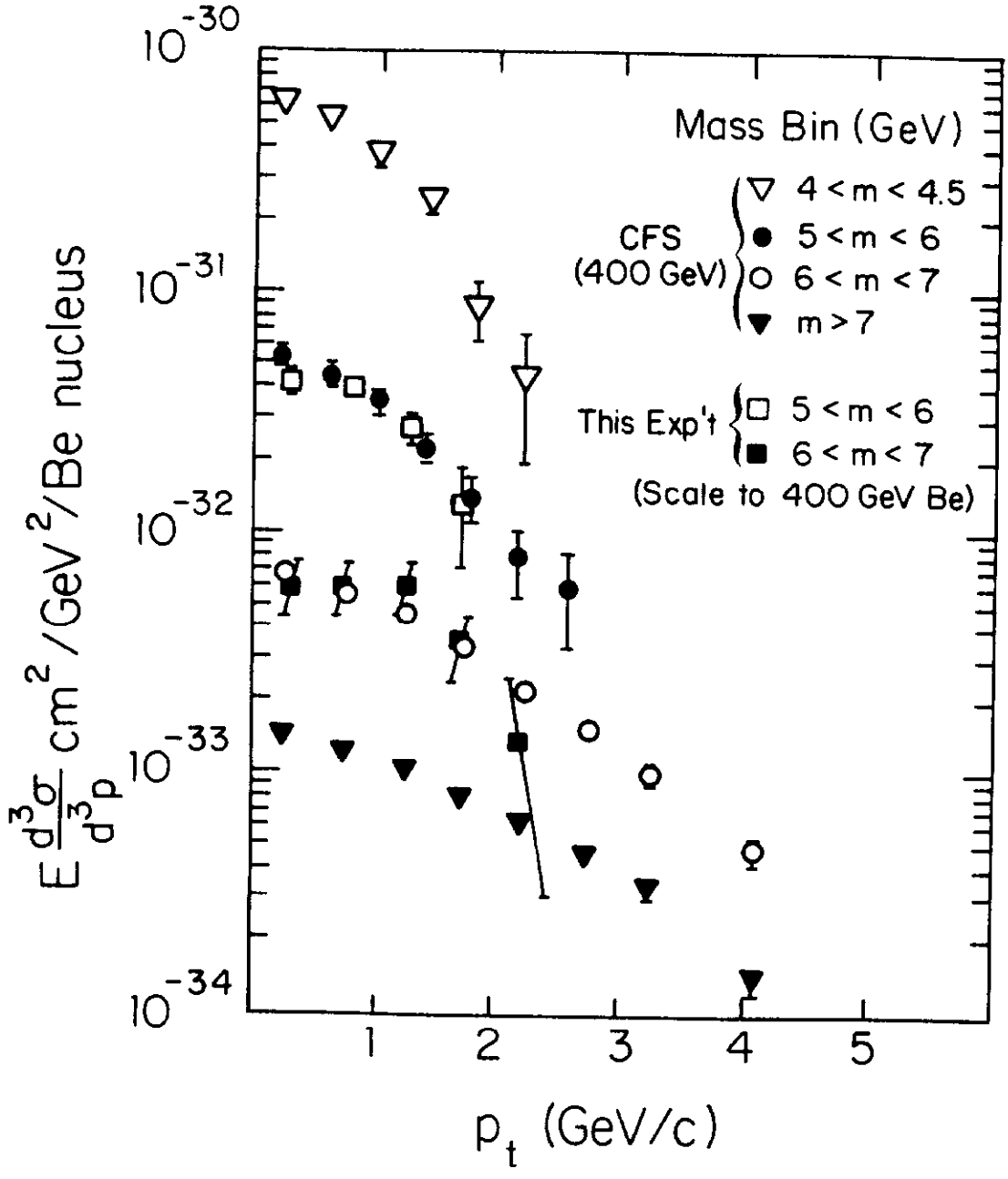
Mass Bin (GeV)
CFS
(400 GeV)
4 < m < 4.5
5 < m < 6
6 < m < 7
m > 7
This Exp't
5 < m < 6
6 < m < 7
(Scale to 400 GeV Be)
$E\frac{d^3\sigma}{d^3p}$ cm^2/GeV^2/Be nucleus
10^{-30}
10^{-31}
10^{-32}
10^{-33}
10^{-34}
1
2
3
4
5
p_t (GeV/c)

Figure 7

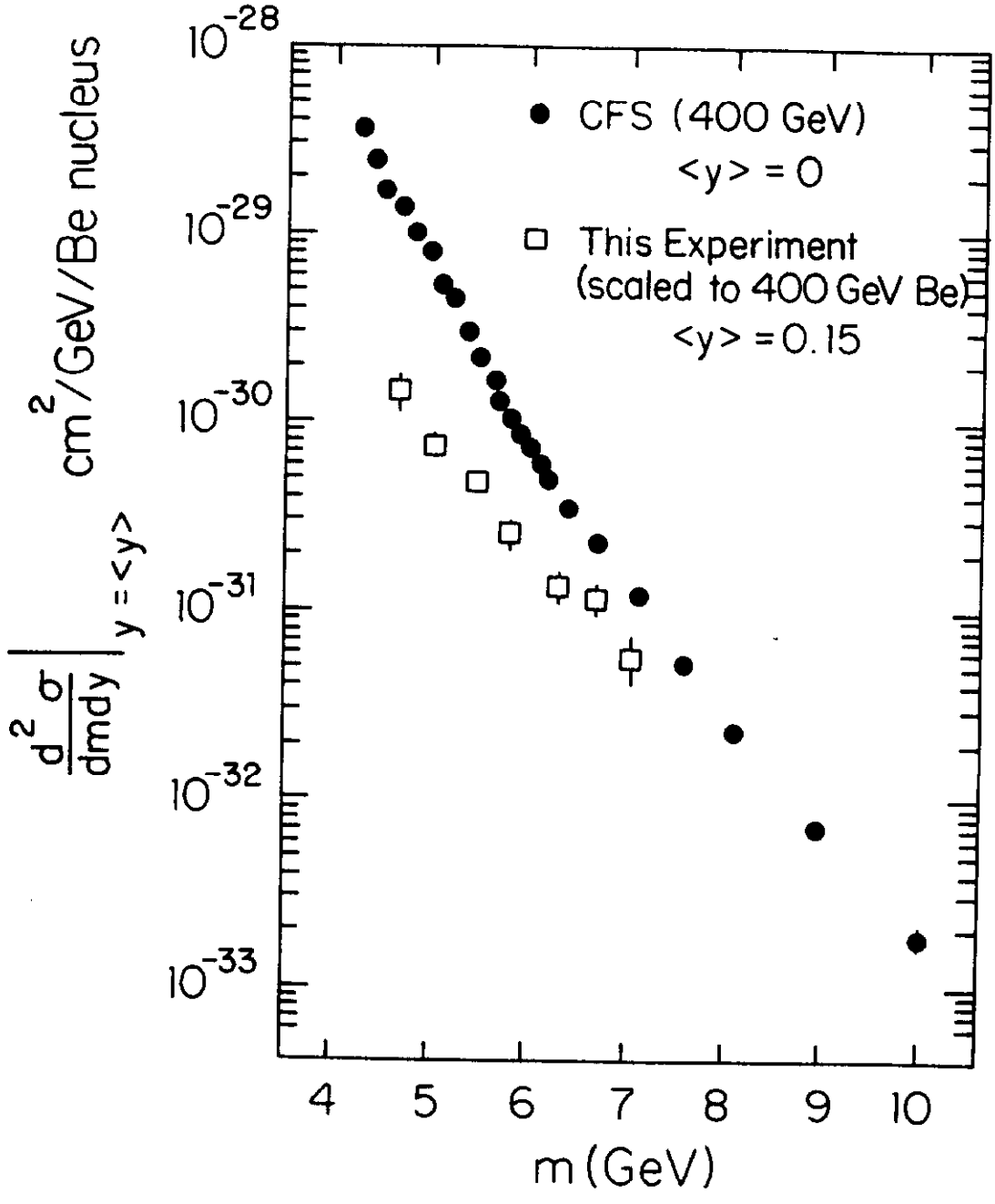
$\frac{d^2\sigma}{dmdy}\Big|_{y=<y>}$ cm^2/GeV/Be nucleus
10^{-28}
10^{-29}
10^{-30}
10^{-31}
10^{-32}
10^{-33}
CFS (400 GeV)
<y> = 0
This Experiment
(scaled to 400 GeV Be)
<y> = 0.15
4
5
6
7
8
9
10
m (GeV)

Figure 8

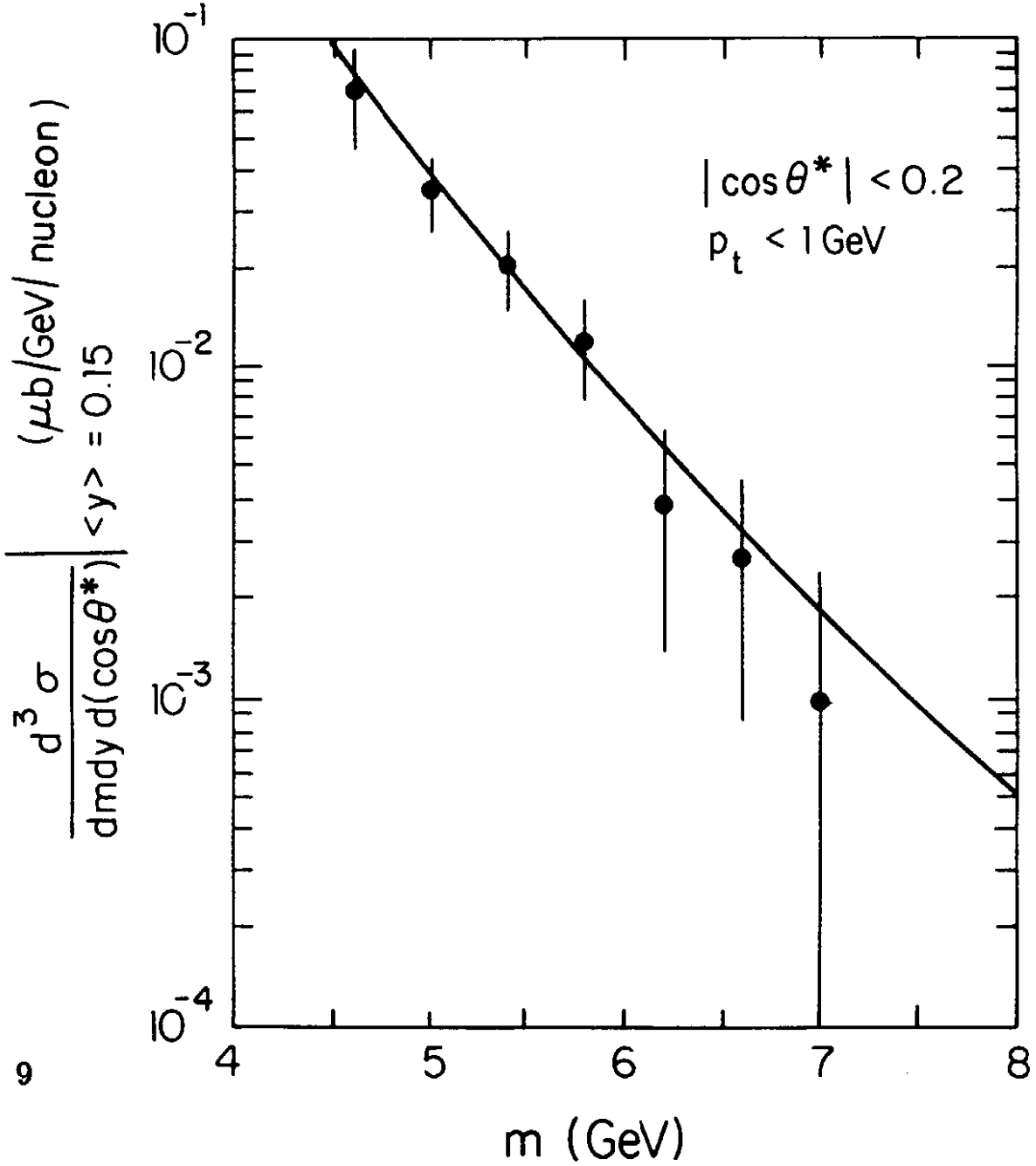
$\frac{d^3\sigma}{dm\,dy\,d(\cos\theta^*)}\Big|_{\langle y\rangle = 0.15}$ (μb/GeV/ nucleon)
10^{-1}
10^{-2}
10^{-3}
10^{-4}
$|\cos\theta^*| < 0.2$
$p_t < 1$ GeV
4
5
6
7
8
m (GeV)

Figure 9

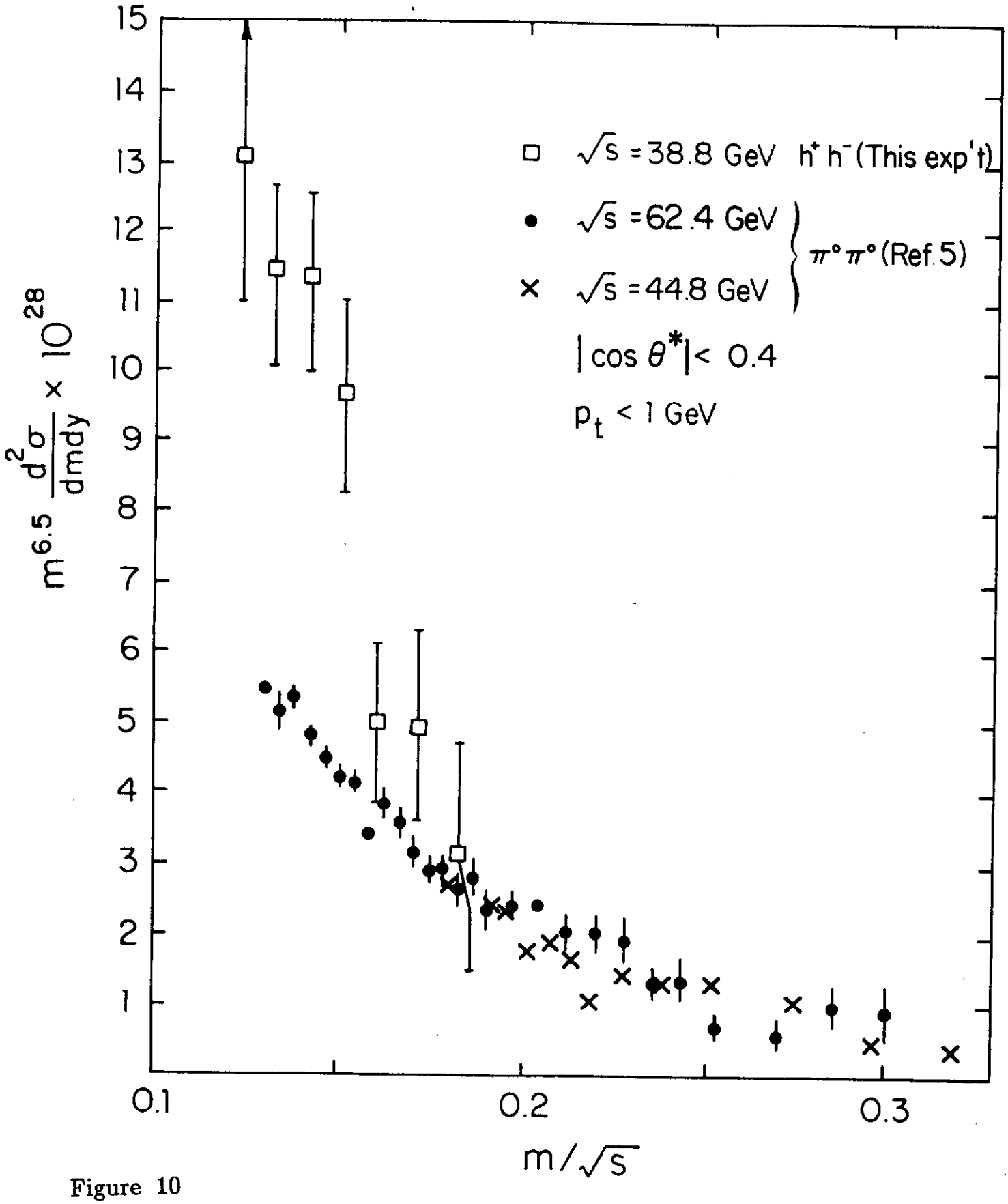
$m^{6.5} \frac{d^2\sigma}{dmdy} \times 10^{28}$
$m/\sqrt{s}$
$\sqrt{s}$ = 38.8 GeV $h^+ h^-$ (This exp't)
$\sqrt{s}$ = 62.4 GeV
$\sqrt{s}$ = 44.8 GeV
$\pi^\circ \pi^\circ$ (Ref. 5)
$|\cos \theta^*| < 0.4$
$p_t < 1$ GeV

Figure 10